Miner Petrol (2011) 103:19–36
DOI 10.1007/s00710-011-0150-1

ORIGINAL PAPER

Magma hybridization in the Western Tatra Mts. granitoid intrusion (S-Poland, Western Carpathians)

Jolanta Burda · Aleksandra Gawęda · Urs Klötzli

Received: 5 December 2010 / Accepted: 6 April 2011 / Published online: 4 May 2011

Abstract In the Variscan Western Tatra granites hybridization phenomena such as mixing and mingling can be observed at the contact of mafic precursors of dioritic composition and more felsic granitic host rocks. The textural evidence of hybridization include: plagioclase–K-feldspar–sphene ocelli, hornblende- and biotite-rimmed quartz ocelli, plagioclase with Ca-rich spike zonation, inversely zoned K-feldspar crystals, mafic clots, poikilitic plagioclase and quartz crystals, mixed apatite morphologies, zoned K-feldspar phenocrysts. The apparent pressure range of the magma hybridization event was calculated at 6.1 kbar to 4.6 kbar, while the temperature, calculated by independent methods, is in the range of 810°C−770°C. U-Pb age data of the hybrid rocks were obtained by in-situ LA-MC-ICP-MS analysis of zircon. The oscillatory zoned zircon crystals yield a concordia age of 368±8 Ma (MSWD=1.1), interpreted as the age of magma hybridization and timing of formation of the magmatic precursors. It is the oldest Variscan magmatic event in that part of the Tatra Mountains.

Editorial handling: A. Möller

J. Burda (✉) · A. Gawęda
Faculty of Earth Sciences, University of Silesia,
Sosnowiec, Poland
e-mail: jolanta.burda@us.edu.pl

U. Klötzli
Department of Lithospheric Research, University of Vienna,
Vienna, Austria

Introduction

Mafic magma has been recognized to play an important role in the process of granite melt generation. The processes of felsic and mafic magma interactions can be observed at different scales: from outcrop scales to micro-chemical and isotopic features. The scale of the observation depends on the range of the process involved: from mixing—where different magmas' identity is not apparent—to mingling, where the individual components from different magmas can be recognized (Menéndez and Ortega 1999, Didier and Barbarin 1991 and references therein). Fundamental features that unequivocally prove the presence of mixing—mingling processes are textural ones.

According to Hibbard (1991), no single texture can be used to prove undoubtedly the presence of hybridization in the granitic rocks, so the term "textural assemblage" was proposed to define the combination of textures, forming together a good proof of mixing—mingling phenomena. Those are as follows: rapakivi and/or antirapakivi texture (Hibbard 1991, Nekvasil 1991), poikilitic crystals of quartz and K-feldspars, sphene-rich ocellar texture (Hibbard 1991, Baxter and Feely 2002), blade "hydrogenic" biotite (Hibbard 1991; Vernon 2004), zoned K-feldspar phenocrysts, with rows of plagioclase, biotite, hornblende etc. inclusions (Vernon 2004, Hibbard 1991; Vernon and Paterson 2008, Słaby et al. 2007a, Słaby et al. 2007b), spike zones in plagioclases and boxy cellular morphology of plagioclase crystals, acicular apatite and mixed apatite morphologies (Hibbard 1991, Baxter and Feely 2002) and small plagioclase laths (Hibbard 1991).

The Western Tatra granitoids (common Tatra type) were formerly interpreted as purely S-type rocks, formed during a prolonged 360–350 Ma magmatic episode (Kohút and Janak 1994; Poller et al. 2001a). In this paper, we discuss the age as well as textural and mineralogical evidences of magma hybridization in the Western Tatra granitoids. The importance of mafic and felsic magma mixing for the formation of the Western Tatra granitoid pluton and the connection to quartz-diorite mafic precursors are also discussed.

Geological setting

The Tatra Mountains are one of the so-called core mountains in the Central Western Carpathians (Fig. 1a), which are uplifted portions of the Variscan crust tectonically emplaced among the Alpine structures of the Carpathian mountain chain. The Tatra Mountains consist of a Variscan crystalline core, overlain by Mesozoic sedimentary formations. The crystalline core comprises composite granitoid intrusion and its metamorphic envelope (Fig. 1b). In the granitoid body four petrographic types of granitoids can be distinguished (Morozewicz 1914; Kohút and Janak 1994). The common Tatra granodiorite-tonalite (S-type) is volumetrically predominant tongue-shaped intrusion, dated at 360–350 Ma (Fig. 1b; Poller et al. 2000, Poller et al. 2001a, b). Quartz-diorites (I-type mingled hybrid, interpreted as magmatic precursors) are present as sills inside the metamorphic envelope, in the border zone of the common Tatra granite (Gawęda et al. 2005) and as enclaves inside the High Tatra (Poller et al. 2001a). High Tatra granite (I/S-type) occurs in the eastern part of the massif (Fig. 1b). It is characterised by the abundance of mafic enclaves and xenoliths of country rocks (Gawęda 2009). The age of that granite body is still problematic: accessible zircon U-Pb data point out ages from 345–335 Ma (Gawęda 2008; Burda 2010) to 314 Ma

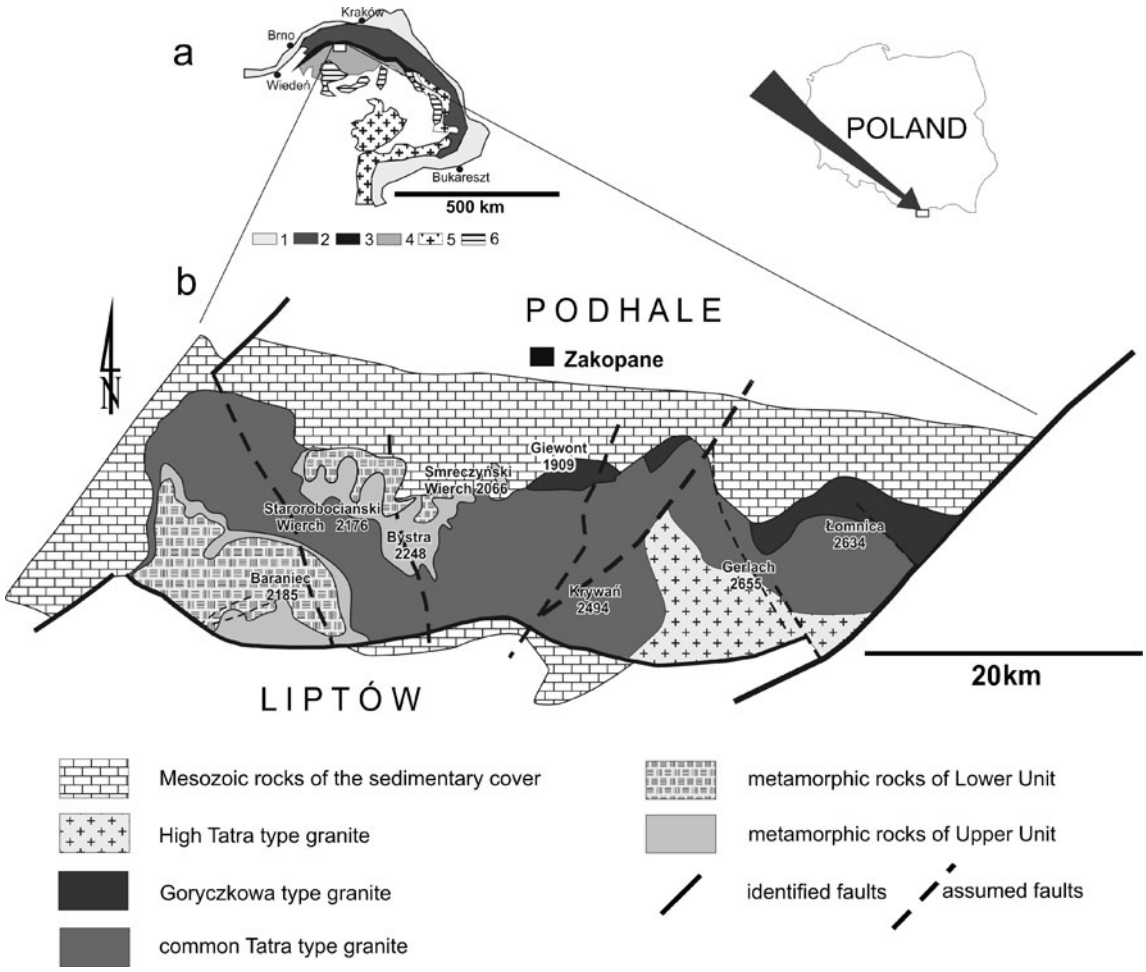

Fig. 1 The geology of the Tatra Mountains. **a** simplified geological sketch of the Carpathian chain. Explanations: 1—Carpathian Foredeep; 2—Outer Carpathians; 3—Pieniny Klippen Belt; 4—Central Western Carpathians; 5—Dacides and South-East Carpathians; 6—Neogene volcanics. **b** geological map of the Tatra Mts block (after Kohút and Janak 1994; Bac-Moszaszwili 1996; Gawęda et al. 2005)

(Poller et al. 2000). Goryczkowa-type granites (S-type), characterised by oriented fabric, were distinguished in the northern part of the crystalline core (Fig. 1b) and dated at 356 Ma (Burda and Klötzli 2007).

Sampling and analytical techniques

Rock samples weighting about 0.5 to 5 kg were collected from the slopes of Staroroboci̇ański Mt, near the contact

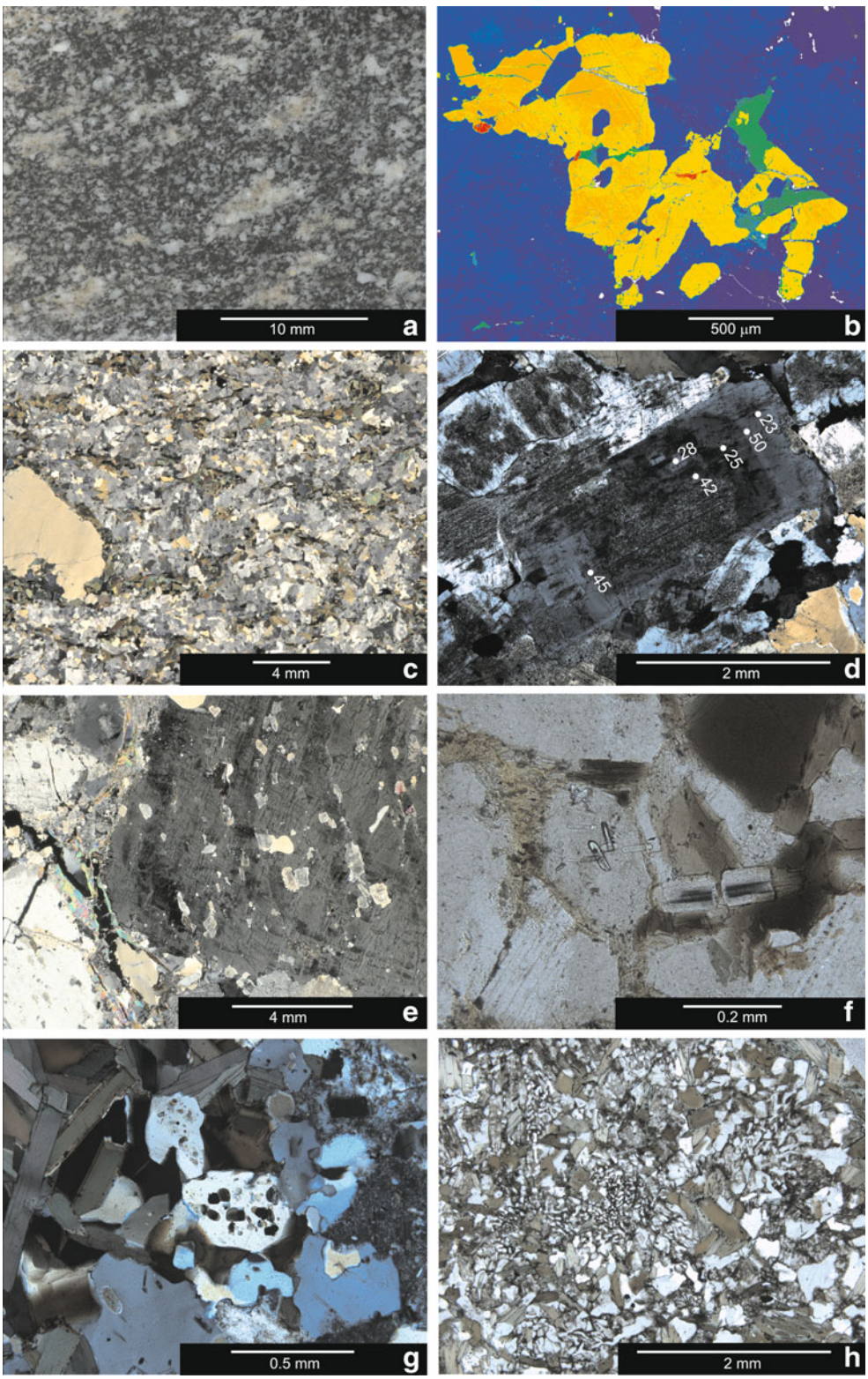

Fig. 2 Textures of hybrid rocks, suggesting mixing-mingling: **a** polished hand-specimen of hybrid rock, showing the presence of numerous plagioclase-sphene ocelli (*light patches*); **b** pseudo-mapping of a fragment of plagioclase-sphene ocellus, with idiomorphic plagioclase crystals (*blue*), intergrown with sphene (*yellow-orange*); **c** microphotograph of quartz-horblende-biotite ocellus in hybrid diorite. Note the presence of elongated mafic clots, crossed nicols; **d** microphotograph of zoned plagioclase crystal, showing calcic spikes, underlined by sericitization; white circles—anorthite content in plagioclase, crossed nicols; **e** microphotograph of a part of K-feldspar phenocryst with inclusion zones, underlying the chemical zonation (see Fig. 4a), crossed nicols; **f** microphotograph of two types of apatite: prismatic with dusty core, broken and seal by biotite, and acicular one, forming inclusions in plagioclase, crossed nicols; **g** microphotograph of the contact zone of diorite (*left*) with granite (*right*) with quartz crystal, poikilitically interlaced with biotite and hornblende, crossed nicols; **h** micrographic texture, composed of quartz and plagioclase, sealing the mafic clots, in the border zone of diorite hybrid, nicols parallel

zone of the common Tatra type granitoid body with the metamorphic country rocks and quartz diorite sill (Fig. 1b). In the investigated rock-sequence three textural varieties of rocks were distinguished: 1—equigranular, relatively mafic (M'=35–28; mafic index M'=Bt+Amph+Ttn+Ep+Opq) biotite and/or amphibole tonalites, fine- to medium-grained; 2—ocellar titanite-rich tonalites and diorites; 3—porphyritic granodiorites-monzogranites with zoned alkali feldspar and plagioclase porphyrocrysts, representing the most felsic variety of the rocks in question.

Mineral analyses were carried out in the Inter-Institution Laboratory of Microanalyses of Minerals and Synthetic Substances, Warsaw (CAMECA SX-100 electron microprobe; 15 kV, 20 nA).

Whole-rock samples were analysed by ICP-ES for major and LILE trace elements and by ICP-MS for HFSE and REE in the ACME Analytical Laboratories, Vancouver, Canada, using sets of internationally recognized standards, according to procedures described on http://acmelab.com. REEs are normalized to C1 chondrite (Sun and McDonough 1989).

Zircon crystals were separated using standard techniques (crushing, hydrofracturing, washing, Wilfley shaking table, Frantz magnetic separator and handpicking). The separation was carried out in the Institute of Geological Sciences, Polish Academy of Sciences, Cracow. Zircon grains were selected for morphological study using scanning electron microscopy and then imaged by panchromatic cathodoluminescence using a FET Philips 30 electron microscope (15 kV and 1 nA) at the Faculty of Earth Sciences, University of Silesia, Sosnowiec, Poland.

Zircon crystals were analysed in the Geochronology Laboratory, Institute of Geology at the University of Vienna. Zircon $^{206}Pb/^{238}U$ and $^{207}Pb/^{206}Pb$ ages were determined using a 193 nm solid state Nd-YAG laser (NewWave UP193-SS) coupled to a multi-collector ICP-MS (Nu Instruments HR). Ablation in a He atmosphere was either spot- or raster-wise according to the zircon CL zonation patterns. Spot analyses were 15–25 μm in diameter whereas rastering line widths were 10–15 μm with a rastering speed of 5 μm/sec. The calculated $^{206}Pb/^{238}U$ and $^{207}Pb/^{206}Pb$ intercept values were corrected for mass discrimination from analyses of standards 91500 (Wiedenbeck et al. 1995) and Plesovice (Slàma et al. 2006) measured during the analytical session. The correction utilizes regression of standard measurements by a quadratic function. A common Pb correction was applied to the final data using the apparent $^{207}Pb/^{206}Pb$ age and the Stacey and Kramers (1975) Pb evolution model. Final U/Pb ages were calculated with 2σ errors using the Isoplot/Ex program, version 3.00 (Ludwig 2003). Details of analytical

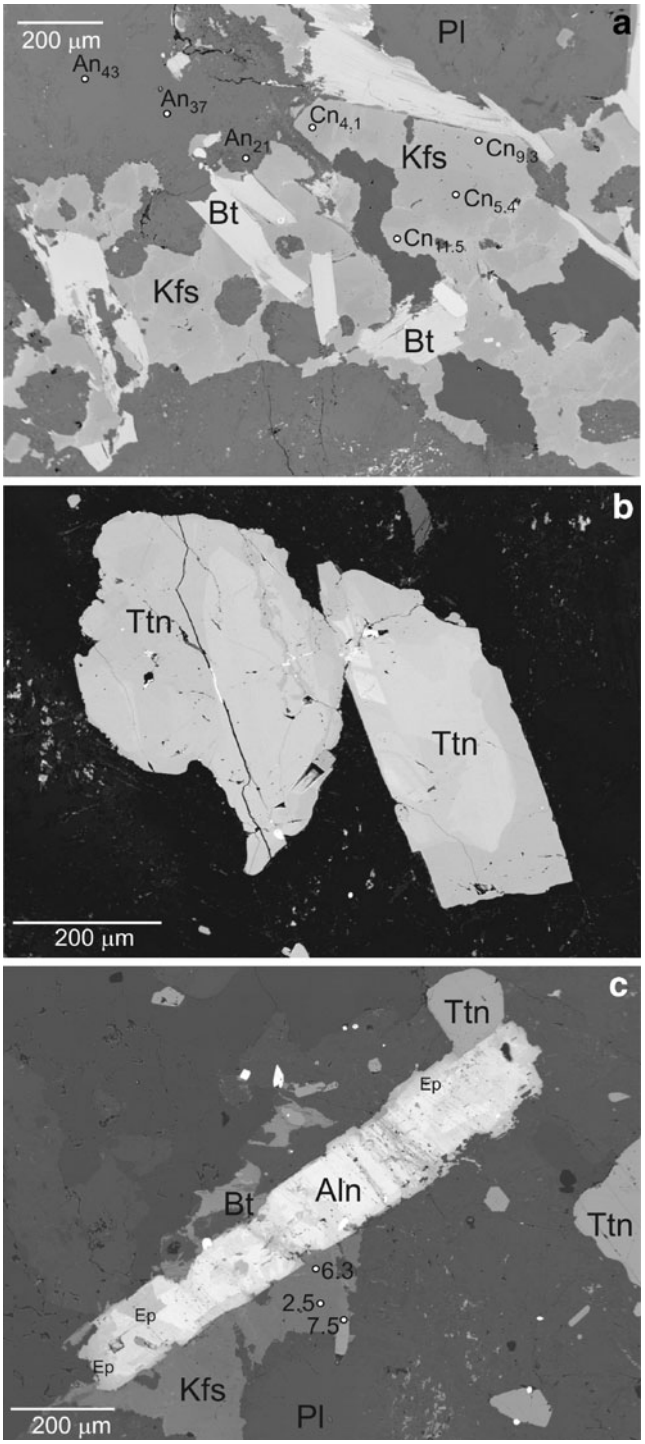

Fig. 3 Back-scattered electron (BSE) images from ocellar hybrid rocks: **a** fine grained matrix, composed of zoned plagioclase crystals (Pl) with marked measured anorthite concentration ($An_{x,y}$=Ca/[Ca+Na+K] * 100%), zoned K-feldspar (Kfs), with marked celsian content ($Cn_{x,y}$=Ba/[K+Na+Ba+Ca] * 100%) and biotite (Bt); **b** titanite crystals showing patchy zoning due to different Al, Fe, Y and Ce substitution (see Table 1); **c** allanite crystal (Aln) from the sphene-rich part of the ocellus, showing the sector zoning to epidote (Ep). It is partly overgrown by sphene (Ttn) and in contact with K-feldspar (Kfs), showing inverted barium zonation (marked celsian content)

procedures and data reduction schemes are given in Klötzli et al. 2009).

Mineral abbreviations used here follow these proposed by Whitney and Evans (2010).

Textures description

Plagioclase-sphene ocellar texture

Plagioclase-sphene ocelli can easily be recognized in diorite-tonalite rocks as lensoidal and spherical light patches up to 0.8 cm in diameter (Fig. 2a, b). Two varieties of this texture were recognised: mafic, with M' at 29 and felsic with M' at 18. Plagioclase-sphene ovoid ocelli are composed of sphene crystals constituting about 18–20 vol.% of the ocelli, in respect to the type of hybrid, usually intergrown with quartz and/or plagioclase crystals, sporadically with apatite inclusions, mantled by plagioclase + quartz + K-feldspar aggregates. Locally, plagioclase crystals forming the ocelli are idiomorphic and show normal zonation with andesine cores (An_{36}-An_{31}) and oligoclase mantles/rims (An_{21}-An_{28}). K-feldspars are xenomorphic and show reverse Ba-zonation ($Cn_{2\text{-}4}$ in the cores and $Cn_{5\text{-}9}$ at rims; Fig. 3a). Sphene crystals, forming the core of the ocelli (Fig. 2b), show patchy zoning (Fig. 3b), due to Al, Fe, Y and Ce substitution in the Ti and Ca sites (Table 1). Locally in the central, sphene-rich part of ocelli, allanite-epidote crystals with sector zoning can be found (Table 2; Fig. 3c).

The ocelli are surrounded by the fine- to medium-grained matrix, composed of plagioclase, biotite and quartz, with accessory K-feldspar, apatite, zircon and opaque minerals, classified as biotite-hornblende quartz-diorite. Two types of biotite crystals could be distin-

Table 1 Selected microanalyses of zoned titanite crystals and their crystal-chemical formulae (20 O^{2-})

Component	Ttn1(r)	Ttn1(c)	Ttn2(r)	Ttn2(m)	Ttn2(c)	Ttn3(s1)	Ttn3(s2)
SiO_2	30.89	31.18	30.10	29.55	29.65	30.32	30.21
TiO_2	36.43	36.83	37.54	36.33	37.53	36.92	36.99
HfO_2	0.30	0.27	0.10	0.26	0.31	0.24	0.28
Al_2O_3	1.21	1.14	1.62	1.32	1.07	1.23	1.44
V_2O_3	0.00	0.39	0.24	0.33	0.41	0.30	0.39
Y_2O_3	0.04	0.06	0.01	0.12	0.14	0.25	0.02
Ce_2O_3	0.67	0.60	0.14	0.62	0.42	0.73	0.29
Nd_2O_3	0.00	0.41	nd	nd	nd	nd	nd
Nb_2O_5	0.20	0.18	0.00	0.28	0.18	0.05	0.05
Ta_2O_5	0.11	0.00	0.28	0.21	0.22	0.19	0.18
FeO	1.12	1.21	0.30	1.22	0.90	1.00	0.32
MnO	0.14	0.13	0.07	0.18	0.10	0.09	0.06
CaO	27.73	27.90	29.00	28.17	28.18	27.16	28.29
Na_2O	0.00	0.02	0.00	0.01	0.02	0.01	0.00
total	98.84	100.21	99.40	98.60	99.13	98.49	98.52
Si	3.585	3.833	3.583	3.581	3.571	3.572	3.618
Ti	3.331	3.200	3.360	3.311	3.400	3.383	3.331
Hf	0.011	0.009	0.011	0.009	0.012	0.008	0.005
Al	0.173	0.155	0.228	0.189	0.152	0.176	0.203
V	0.000	0.037	0.023	0.032	0.039	0.028	0.037
Y	0.002	0.004	0.001	0.008	0.008	0.016	0.001
Ce	0.030	0.026	0.006	0.028	0.018	0.033	0.013
Nb	0.013	0.011	0.000	0.018	0.011	0.003	0.003
Ta	0.004	0.000	0.009	0.007	0.007	0.006	0.006
Fe	0.114	0.117	0.030	0.124	0.090	0.102	0.032
Mn	0.014	0.026	0.007	0.018	0.008	0.009	0.007
Ca	3.612	3.453	3.697	3.658	3.637	3.546	3.630
Na	0.000	0.004	0.000	0.002	0.004	0.002	0.000

Table 2 Representative microanalyses and crystal-chemical formulae (25 O^{2-}) of allanite-epidote minerals

Component	All(s1)	All(s2)	All(m1)	Al(m2)	Ep(r)
SiO_2	31.66	33.40	32.13	34.94	37.31
TiO_2	0.47	0.73	0.69	0.18	0.01
ThO_2	0.88	1.34	1.14	0.55	0.02
Al_2O_3	16.01	17.20	16.33	22.71	21.66
Fe_2O_3	15.47	13.43	15.24	9.77	16.01
La_2O_3	4.03	6.28	6.49	2.68	0.00
Ce_2O_3	9.05	8.70	8.79	5.54	0.08
Pr_2O_3	0.95	0.58	0.60	0.56	0.00
Nd_2O_3	4.05	1.58	1.64	2.03	0.00
Sm_2O_3	0.44	0.20	0.15	0.19	0.00
MgO	1.05	0.56	0.68	0.17	0.00
MnO	0.39	0.55	0.33	0.15	0.00
CaO	12.22	11.90	13.91	18.28	22.66
P_2O_5	0.31	0.16	0.00	0.36	0.29
Total	98.98	96.62	98.12	98.11	98.04
Si	6.348	6.083	6.101	6.040	6.219
Ti	0.105	0.067	0.098	0.023	0.002
Th	0.058	0.038	0.049	0.022	0.001
Al	3.853	3.625	3.654	4.626	4.255
Fe	1.658	2.164	2.102	1.269	1.952
La	0.440	0.286	0.454	0.171	0.000
Ce	0.605	0.637	0.611	0.351	0.005
Pr	0.040	0.067	0.041	0.035	0.000
Nd	0.107	0.278	0.112	0.125	0.000
Sm	0.013	0.029	0.010	0.011	0.000
Mg	0.047	0.158	0.192	0.045	0.000
Mn	0.063	0.090	0.053	0.023	0.000
Ca	3.296	2.424	2.830	3.385	4.000
P	0.026	0.051	0.000	0.052	0.002
Fe/(Fe+Al)	0.301	0.374	0.365	0.215	0.314
ΣREE	1.205	1.297	1.228	0.693	0.005

guished here: blade-shape "hydrogenic" biotite (sensu Hibbard 1991), characterised by Ti contents of about 0.37–0.39 a.p.f.u. (*atoms per formula unit*), found in the vicinity of ocelli, and "platy" biotites, present elsewhere in the matrix, showing Ti content of 0.31–0.34 a.p.f.u. (Table 3). Plagioclase, found in the matrix, is generally oligoclase-andesine in composition (An_{21-37}) but the zonation patterns are complicated by the calcic spikes (An_{41}-An_{50}). Remnants of hornblende, partly replaced by chlorite, are classified as ferro-edenitic hornblende to ferro-hornblende in the cores with actinolitic hornblende or actinolite at rims (Table 4).

Hornblende and biotite rimmed quartz ocelli

These are present in medium-grained, hornblende-bearing granite varieties. The ocelli consist of a quartz core rimmed by ferro-edenitic hornblende (Table 4) and/or biotite. The diameter of the ocelli reach 2.5 cm in length (Fig. 2c).

Plagioclase crystals with spike zoning

In all investigated rocks the presence of plagioclase crystals was noted, mostly of oligoclase composition, showing the sharp compositional discontinuities (calcic spikes) in the range An_{40-50} (Fig. 2d). This texture was described originally by Wiebe (1968) and then found in many magmatic rocks (i.e. Hibbard 1991, Baxter and Feely 2002) where it was attributed to magma mixing process. The exception is the matrix surrounding the titanite ocelli, where plagioclase crystals are generally more calcic (An_{30-50}), showing normal zonation.

K-feldspar phenocrysts with inclusion zones

Coarse-grained porphyritic granite contains both normal and reversely zoned K-feldspar phenocrysts, sporadically mantled by albite, sometimes with resorption features at the border (Fig. 2e). In the K-feldspar phenocrysts the zones of inclusions are abundant, underlying the chemical zonation. Normally zoned phenocrysts have 3.7–5.2 at% of celsian component in the core and 1.5–2.0 at% in the mantle, with a local increase up to 3.1 at% celsian at the rim (Fig. 4a). The celsian contents in the reversely zoned phenocrysts change from 0.7–1.35 at% in the core, 0.5–1.1 at% in the mantle (with local peaks at 1.5–1.8, following the plagioclase rows, attached by synneusis (sensu Vernon 2004) to 2.3–2.6 at% near the margin (Fig. 4b). Such changes in Ba content could be understand in terms of mixing of more felsic, Ba-poor magma with mafic, Ba-enriched, more oxidized magma (Long and Luth 1986; Słaby and Galbarczyk-Gąsiorowska 2002; Słaby and Götze 2004).

Mafic clots

The border zone at the contact of quartz-diorite with granite is composed of mafic aggregates ("clots"), 2–6 mm in diameter, included in the felsic matrix. The matrix represents the quenched melt, and shows a micrographic texture (Fig. 2h) composed of quartz and plagioclase (An_{25-29}), locally antiperthitic. The mineral components of mafic clots are: biotite, hornblende, opaque

Table 3 Representative microanalyses of biotite from hybrid granitoids (G) and diorites (D) and their crystal-chemical formulae (22 O^{2-})

Component	BtG1(bl)	BtG2(c)	BtG2(m)	BtG4 (bl)	BtG5(c)	BtG5(m)	Bt-D(1)	Bt-D(2)
SiO_2	36.10	35.94	35.78	35.92	35.43	36.09	38.23	35.84
TiO_2	3.17	3.21	2.84	2.93	2.70	3.35	2.81	2.75
Al_2O_3	15.20	15.57	15.21	15.42	15.95	15.46	14.63	16.77
MgO	9.81	9.86	9.79	9.44	9.26	9.31	14.16	11.12
MnO	0.27	0.35	0.28	0.16	0.13	0.28	0.25	0.22
FeO	21.15	20.08	21.13	21.66	21.13	20.46	15.13	17.99
BaO	0.37	0.22	0.06	0.45	0.35	0.12	0.38	0.26
Na_2O	0.10	0.12	0.08	0.08	0.17	0.11	0.11	0.10
K_2O	9.22	9.41	9.35	9.56	9.23	9.21	9.48	9.63
Total	95.39	94.76	94.52	95.62	94.45	94.39	95.18	94.68
Si	5.573	5.555	5.571	5.556	5.531	5.598	5.728	5.490
Al^{IV}	2.427	2.445	2.429	2.444	2.469	2.402	2.272	2.510
Al^{VI}	0.339	0.391	0.362	0.368	0.466	0.424	0.311	0.518
Ti	0.368	0.373	0.332	0.341	0.317	0.391	0.317	0.317
Mg	2.257	2.272	2.273	2.177	2.155	2.152	3.162	2.539
Mn	0.035	0.046	0.036	0.021	0.017	0.036	0.032	0.029
Fe	2.730	2.596	2.752	2.802	2.759	2.653	1.896	2.304
Ba	0.022	0.014	0.004	0.027	0.021	0.007	0.023	0.015
Na	0.030	0.036	0.025	0.024	0.051	0.033	0.033	0.029
K	1.817	1.855	1.858	1.886	1.837	1.823	1.811	1.882
fm	0.551	0.538	0.551	0.565	0.563	0.555	0.379	0.479

Explanations: *bl* blade-shape, *c* core, *m* margin, *fm* $Fe^{+2}/(Fe^{+2}+Mn+Mg)$

minerals (ilmenite-magnetite exsolution), allanite, and locally pseudomorphs after pyroxene.

Mixed apatite morphologies

Two generations of apatite 1) prismatic, with dusty cores, and 2) acicular (Fig. 2f) could be found in all the lithological types of magmatic rocks, including the plagioclase-sphene ocelli. Prismatic, zoned apatites (sometimes broken; Fig. 2f) represent the earlier crystallization episode from the fractionated magma. The acicular apatite crystals crystallized as a result of mafic magma quenching (especially when enriched in phosphorus). The presence of acicular apatite alone was thought to be one of the textures typical of magma mixing (Hibbard 1991), but the coexistence of two different apatite morphologies might be also explained by magma mixing—mingling process (Baxter and Feely 2002).

Poikilitic plagioclase and quartz crystals

The albitic plagioclase and quartz crystals, full of biotite, hornblende, and K-feldspar inclusions, are present in all lithologies in the mixing-mingling zone, but they are especially abundant at the contact of granite with diorite and inside the quenching zone (Fig. 2g).

Hybrid rocks chemistry

The hybrid rocks are peraluminous in composition (ASI>1.1; Fig. 5a; Tables 5 and 6) subalkaline (Fig. 5b) and intermediate in Mg-number (#mg=0.42–0.78; Tables 5 and 6). They plot in the high-K calc-alkaline field of the K_2O versus SiO_2 diagram (Fig. 5c). Generally hybrids show variable predominance of sodium over potassium (Na_2O/K_2O=1.0–1.9). More felsic lithologies sporadically show K_2O enrichment (Na_2O/K_2O= 0.6–0.9). Following the major elements, Rb/Sr ratios are low to moderate (0.08–0. 68, Fig. 5d; Tables 5 and 6). On the triangular Q-Ab-Or diagram analysed samples of hybrid granitoids plot mostly close to quartz-feldspars cotectics for pressures between 2–5 kbar, while ocellar hybrids plot near the cotectic for 10 kbar, forming a linear trend towards the quartz-diorites (Fig. 6). The hybrid

Table 4 Microprobe analyses and crystal-chemical formulae of amphiboles (13-CNK) from hybrid rocks

Sample	A1(c)	A1(m)	A3(m1)	A3(m)	A3(m2)	A5(c)	A5(m)	A8(c)	A8(m)
SiO_2	45.42	49.30	45.39	44.78	44.76	44.01	45.00	44.69	46.12
TiO_2	0.87	0.44	0.84	1.00	0.87	0.98	0.99	0.97	0.82
Al_2O_3	7.70	5.42	8.36	9.86	8.26	9.28	8.75	8.85	7.21
FeO	18.37	17.37	18.49	18.71	18.54	18.97	19.03	19.13	18.90
MnO	0.49	0.53	0.54	0.52	0.52	0.50	0.42	0.47	0.51
MgO	9.40	11.07	9.34	8.93	9.05	8.69	9.14	8.95	9.57
CaO	11.91	11.91	11.58	11.65	11.81	11.71	11.70	11.79	11.89
Na_2O	1.04	0.47	0.97	1.19	0.91	1.00	1.18	1.08	0.72
K_2O	0.72	0.38	0.78	0.99	0.85	1.00	0.92	0.97	0.74
Total	95.92	96.89	96.29	97.63	95.57	96.14	97.13	96.90	96.48
Si	6.974	7.373	6.935	6.764	6.909	6.780	6.846	6.828	7.039
Al^{iv}	1.026	0.627	1.065	1.236	1.091	1.220	1.154	1.175	0.975
Al^{vi}	0.367	0.329	0.440	0.519	0.411	0.466	0.416	0.419	0.320
Fe^{+3}	0.010	0.000	0.000	0	0.047	0.049	0	0.026	0.113
Ti	0.101	0.049	0.096	0.114	0.101	0.113	0.114	0.112	0.094
Mg	2.152	2.469	2.128	2.011	2.083	1.995	2.072	2.039	2.178
Fe^{+2}	2.359	2.172	2.363	2.363	2.393	2.444	2.421	2.444	2.413
Mn	0.064	0.067	0.070	0.066	0.068	0.065	0.054	0.061	0.065
Ca	1.959	1.909	1.896	1.885	1.953	1.932	1.908	1.930	1.944
Na	0.310	0.135	0.287	0.349	0.274	0.298	0.349	0.318	0.212
K	0.140	0.072	0.151	0.190	0.168	0.196	0.178	0.189	0.144
#mg	0.477	0.532	0.474	0.460	0.465	0.449	0.461	0.455	0.474
name	Fe-Hbl	Act-Hbl	Fe-Hbl	Fe-Ed	Fe-Hbl	Fe-Hbl	Fe-Ed	Fe-Ed	Fe-Hbl

Explanations: *c* core; *m* margin, *#mg* $Mg/(Fe^{+2} + Mg)$

quartz-diorites (mafic precursors) are metaluminous in composition, plot in the lower part of sub-alkaline field, and are characterised by extremely low Rb/Sr ratios (Figs. 5a, b, d; Table 5).

On variation diagrams TiO_2, Fe_2O_3 and CaO hybrid granitoids and quartz diorites form one linear trend (Figs. 5e, g, h), while ASI, Al_2O_3 and P_2O_5 of these rocks form two different trends, crossing in the area of samples rich in titanite-feldspar ocelli (Figs. 5a, f, i).

Chondrite (C1)-normalized REE patterns show either negative or almost no Eu anomalies (Eu/Eu*=0.62–1.05), except for the porphyritic granite with a positive Eu anomaly (Eu/Eu*=1.24). The REE fractionation is very variable: from low (Ce_N/Yb_N=4.5–10) to high (27.3–55.6; Fig. 7a, b; Table 5 and 6). The quartz diorites present in the same area (Gawęda et al. 2005) are characterised by weakly negative or lack of Eu anomaly (Eu/Eu*=0.777–1.065) and moderate REE fractionation (Ce_N/Yb_N=12.72–18.04; Table 5; Fig. 7a, b–grey shadow area for comparison).

Temperature and pressure calculations

The application of Schmidt (1992) hornblende geobarometry calibration (Table 7) gives an apparent pressure range of 6.1 kbar to 4.6 kbar, in accordance with earlier results obtained for quartz diorites from the same area (Gawęda et al. 2005). Temperature of crystallization was calculated using the Blundy and Holland (1990) geothermometric calibration and comparatively, the Vyhnal et al. (1991) calibration as well as the similar calibration proposed by Gawęda (2009). Ternary feldspars geothermometry (Fuhrman and Lindsley 1988; Nekvasil and Burnham 1987) was applied, giving the disequilibrium temperatures, although plotting in the narrow range of 695°C to 738°C for assumed 4–6 kbar of pressure (Table 7). Anti-perthites, found in the micrographic texture were also used to calculate the exsolution equilibrium temperatures, using ternary feldspars geothermometry, and point out the range of 551-568°C. The whole rock Zr contents were used to calculate the magma temperature

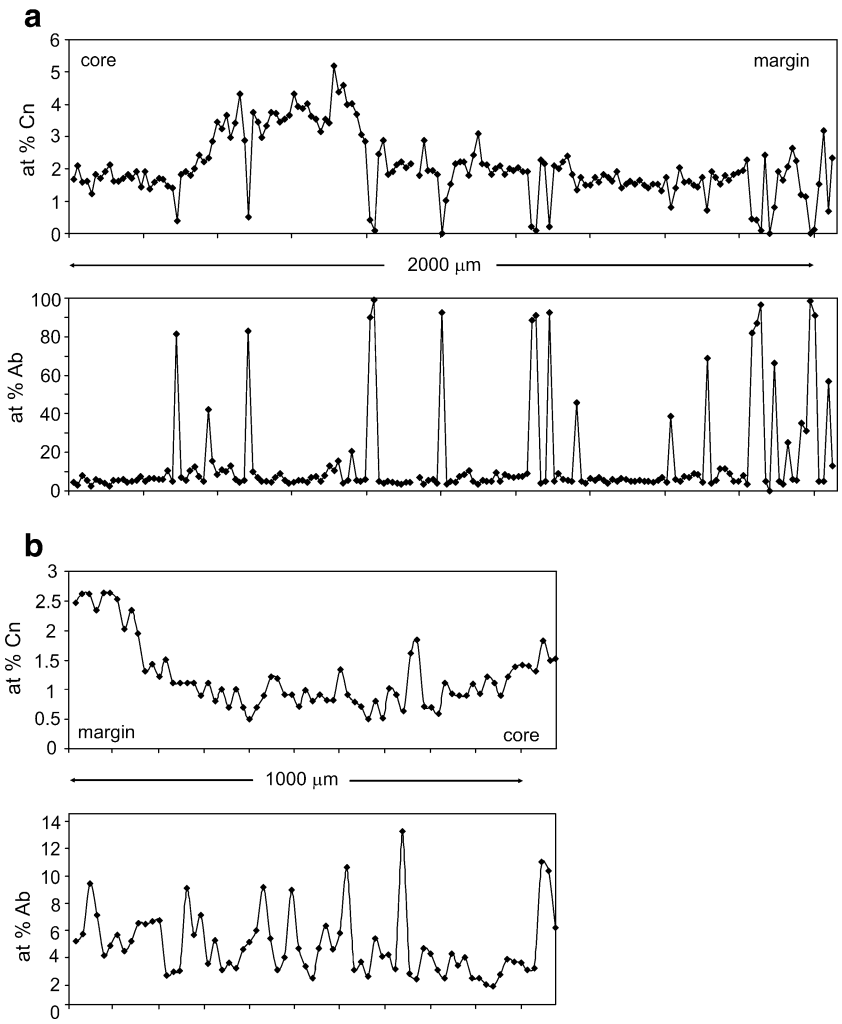

Fig. 4 Two examples of celsian (Cn) and albite (Ab) components distribution in alkali feldspar phenocrysts from hybrid rocks: **a** K-feldspar showing the normal barium zoning, expressed as celsian content (at % Cn), underlined by plagioclase rows, attached by synneusis, expressed as peaks of albite (Ab) content; **b** K-feldspar with inverted barium zoning, with no inclusions of plagioclase. Celsian atomic percent (at% Cn) calculated as Ba/(K+Ba+Na+Ca) * 100% from alkali feldspar formula

(Harrison and Watson 1983), which plot in the bracket of 810°C–770°C.

Zircon characteristics and geochronology

Zircon crystals from the hybrid granitoid showing ocellar textures (sample SP2; Table 6) were selected for dating. Crystals are clear and colourless to pale yellow. Zircons are typically 200–300 μm in length, euhedral, short to long prismatic, with aspect ratios of 1:2 to 1:5 (Fig. 8). There are two morphological types of crystals. Type 1 shows a predominance of [110] prism forms and the presence of two pyramids [101, 211] with the latter more dominant (subtypes S2, S6, S7 in Pupin's typological classifications; Fig. 9). This morphological type is characteristic for zircon crystals from S-type aluminous granitoids (Pupin 1980). Type 2 zircons have a well-developed [110] prism and [101] pyramid forms (subtypes S5, L5, L4; Fig. 9). According to the genetic classification (Pupin 1980) this type is typical for zircon from sub-alkaline and alkaline series granitoids of crustal plus mantle or mainly mantle origin.

Some zircon grains revealed intermittent dissolution surfaces between well-developed oscillatory zoning (Fig. 10). These might fingerprint the corrosion or resorption events during evolution of zircon crystals (e.g. Vavra 1990, Köksal et al. 2008). Some grains exhibit homogeneous to weakly growth-zoned cores with bright luminescence surrounded by euhedral overgrowths with oscillatory zoning. Zircon cores are sub-rounded and the contacts with surrounding oscillatory-zoned rims are irregular. Locally, recrystallization patches (loss of oscillatory zoning) are also present (Fig. 10).

Microprobe analyses were performed on zircon sections polished parallel to the c axis. In analysed grains oscillatory zoning of HfO_2 is visible (Table 8). A positive correlation between P and Y, suggesting the xenotime-type

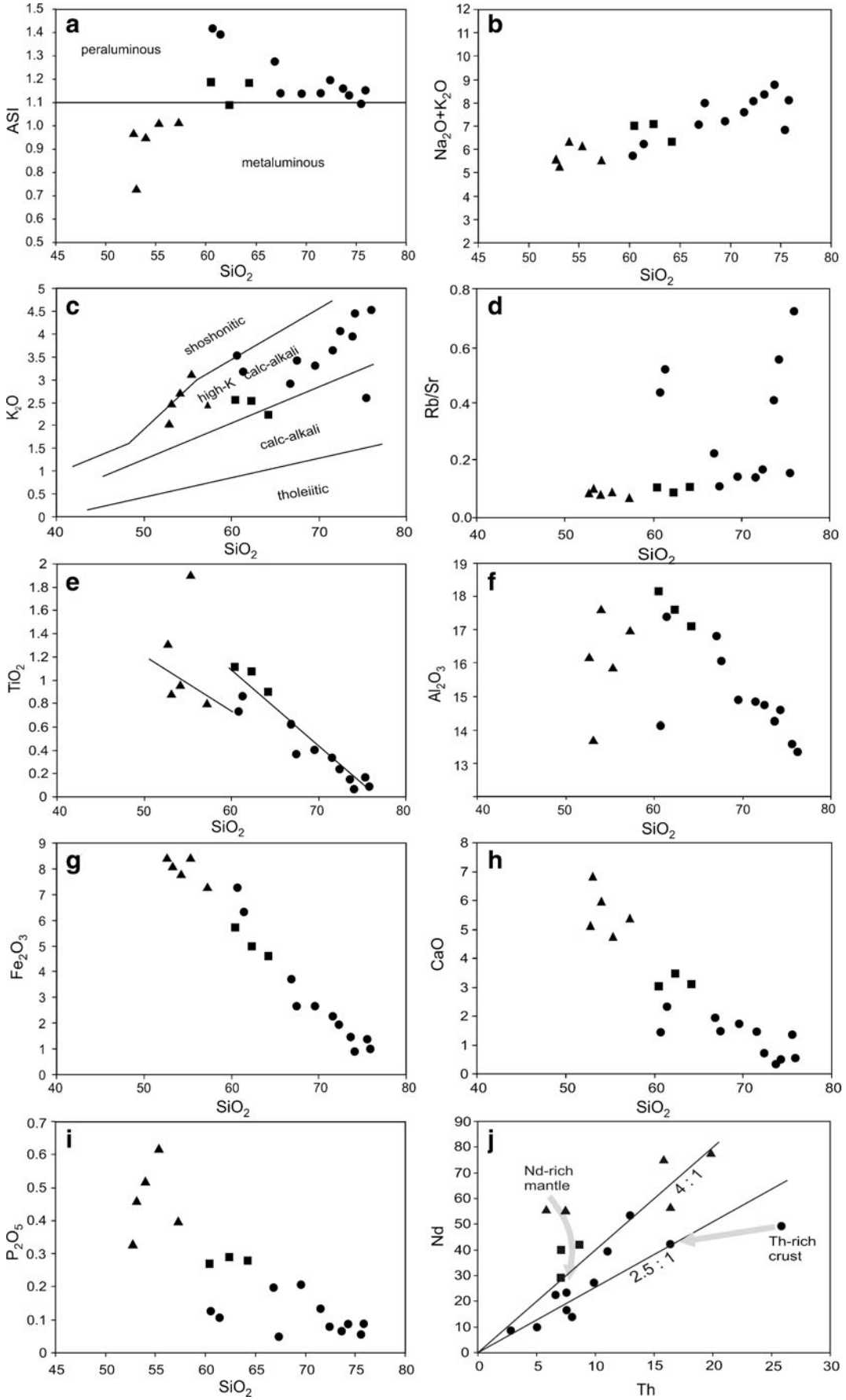
a
peraluminous
metaluminous
ASI
SiO2
b
Na2O+K2O
SiO2
c
shoshonitic
high-K calc-alkali
calc-alkali
tholeiitic
K2O
SiO2
d
Rb/Sr
SiO2
e
TiO2
SiO2
f
Al2O3
SiO2
g
Fe2O3
SiO2
h
CaO
SiO2
i
P2O5
SiO2
j
Nd-rich mantle
4 : 1
2.5 : 1
Th-rich crust
Nd
Th

◀ **Fig. 5** Variation diagrams for ASI **a** and major elements **b**, **c**, **e**–**i** versus SiO_2, Rb/Sr versus SiO_2 **d** and Nd versus Th **j** of the hybrid granitoids (*circles*), ocellar hybrids (*squares*) and quartz-diorites (*triangles*)

substitution $Zr^{4+}+Si^{4+}\leftrightarrow(Y, REE)^{3+}+P^{5+}$ (Speer 1982), is observed. The crystal domains with oscillatory zoning are characterized by Zr/Hf ratios in the range of 35–52 and Th/U>0.1 (Table 8).

Table 5 Chemical composition and selected petrological indicators of hybrid granitoids from the Western Tatra Mountains

Sample	Gh1	Gp1	H4p	Gp2	Gh2	Gh3	Gp3	Gp4	Gh4	Gh5
SiO_2	72.42	75.52	73.72	72.72	71.54	69.58	74.27	75.95	66.89	61.44
TiO_2	0.22	0.15	0.13	0.24	0.31	0.38	0.07	0.11	0.6	0.84
Al_2O_3	14.68	13.5	14.3	14	14.72	14.8	14.52	13.37	16.78	17.45
Fe_2O_{3T}	1.86	1.31	1.38	1.77	2.24	2.57	0.79	1.03	3.58	6.23
MnO	0.04	0.03	0.03	0.03	0.04	0.05	0.02	0.01	0.05	0.09
MgO	0.53	0.42	0.55	0.5	0.94	1.31	0.22	0.19	1.38	3.28
CaO	0.75	1.39	0.41	0.74	1.49	1.77	0.56	0.6	1.98	2.37
Na_2O	4.08	4.28	4.53	2.89	4.03	4.02	4.37	3.51	4.12	3.03
K_2O	4.01	2.62	3.93	6.1	3.58	3.29	4.4	4.54	2.92	3.17
P_2O_5	0.08	0.06	0.07	0.09	0.14	0.21	0.09	0.09	0.2	0.11
LOI	1	0.8	0.8	0.6	1.1	1	0.7	0.7	1.9	2.3
Total	99.67	100.11	99.85	99.68	100.13	98.98	100.01	100.1	100.4	100.31
Sr	458.4	419.4	208.2	287.8	556.2	596.3	169.8	136.3	456.9	278
Ba	1418	697	566	1863	1708	1528	802	756	759	809
Rb	72.6	62.5	81.6	114.7	78.3	86.8	89.4	92.7	98.7	137
Th	7.5	2.9	7.7	16.5	25.9	16.5	8.1	5.2	9.8	6.7
U	1	1.3	1.5	2.7	2.9	2.5	1.8	2.1	1.5	1.6
Ga	15.3	14.7	16	14.6	19.9	20.6	13.5	14.5	20.2	18.7
Zr	107.1	70.2	100.9	144.7	174.3	169.6	52.7	64.8	140.6	185.2
Hf	3.4	2.1	3.2	4.7	5.6	5.3	2.1	2.7	4	4.6
Y	18.1	6.5	3.5	9.7	8	10.4	16.8	15.8	11.6	18.6
Nb	3.8	2.7	5.6	4.9	5.3	6.6	4	4.7	7	9.7
Ta	0.3	0.3	0.6	0.3	0.2	0.3	0.3	0.5	0.4	0.5
La	25	10.3	19.1	36.2	55.4	46.4	14	9	28.8	22.9
Ce	52.1	21.7	40.3	83.9	119	100.5	32.3	20.5	61.6	49.6
Pr	6.04	2.44	4.62	9.59	13.34	11.28	3.67	2.4	7.5	5.48
Nd	23.6	9.3	16.6	38	49.1	42.3	14.4	9.5	27.1	22.6
Sm	4.21	1.64	2.69	7.26	7.35	7.1	3.17	2.11	4.43	4.09
Eu	1.06	0.61	0.58	1.01	1.31	1.24	0.6	0.54	0.97	1.21
Gd	3.46	1.39	1.71	4.7	4.25	4.18	2.9	2.2	3.13	3.87
Tb	0.55	0.22	0.21	0.59	0.47	0.51	0.5	0.44	0.43	0.6
Dy	3.03	1.22	0.76	2.21	1.69	2.27	2.88	2.5	2.39	3.36
Ho	0.61	0.23	0.11	0.26	0.23	0.32	0.54	0.51	0.41	0.64
Er	1.7	0.63	0.27	0.68	0.65	0.81	1.56	1.44	1.09	1.9
Tm	0.24	0.1	0.05	0.09	0.09	0.12	0.22	0.21	0.16	0.28
Yb	1.44	0.65	0.26	0.62	0.59	0.78	1.35	1.26	0.89	1.84
Lu	0.2	0.09	0.05	0.08	0.09	0.11	0.21	0.18	0.13	0.29
ASI	1.201	1.101	1.164	1.121	1.143	1.148	1.138	1.156	1.285	1.4
#mg	0.34	0.36	0.42	0.33	0.43	0.48	0.33	0.25	0.41	0.48
Na_2O/K_2O	5.44	3.08	1.15	3.91	1.13	1.22	7.8	0.77	1.41	1.28
Rb/Sr	0.158	0.149	0.392	0.399	0.141	0.146	0.526	0.68	0.216	0.493
Nd/Th	3.147	3.207	2.156	2.303	1.896	2.564	1.778	1.827	2.765	3.373
ΣREE	123.24	50.52	87.31	185.19	253.56	217.92	78.3	52.79	139.03	118.66
Eu/Eu*	0.849	1.235	0.827	0.529	0.717	0.696	0.605	0.766	0.796	0.93
Ce_N/Yb_N	9.969	9.198	42.707	37.285	55.572	35.501	6.592	4.483	19.07	7.427

Explanations: *Gh* homogeneous granitoids, *Gp* pophyritic granitoids, *Hp* hybrids with K-feldspar porphyrocrysts, *#mg* $Mg/(Fe^{+2}+Mg)$

Table 6 Chemical composition of selected hybrid granitoid and quartz-diorite rocks from the Western Tatra Mountains

Sample	GH2a	GH2b	H1(M)	H2(F)	SP2(H)	D1-WT	D2-WT	D3-WT	D4-WT
SiO_2	67.47	60.7	62.38	60.51	64.23	52.75	55.32	53.08	54.01
TiO_2	0.36	0.75	1.05	1.08	0.87	1.29	1.88	0.86	0.94
Al_2O_3	16.01	14.08	17.54	18.12	17.04	16.1	15.81	13.62	17.55
Fe_2O_{3T}	2.56	7.15	5.09	5.83	4.71	8.36	8.36	8.16	7.58
MnO	0.05	0.13	0.07	0.09	0.05	0.14	0.13	0.14	0.12
MgO	1.65	6.73	2.04	2.31	1.8	7.47	3.46	9.42	5.77
CaO	1.51	1.49	3.53	3.09	3.17	5.19	4.83	6.92	6.05
Na_2O	4.6	2.21	4.58	4.51	4.15	3.58	3.09	2.86	3.67
K_2O	3.44	3.54	2.48	2.5	2.17	2.01	3.08	2.43	2.67
P_2O_5	0.05	0.13	0.29	0.27	0.28	0.33	0.62	0.46	0.52
LOI	1.5	2.5	1.2	1.8	1.3	3.01	2.62	2.47	1.41
Total	99.2	99.41	100.25	100.11	99.77	100.23	99.2	100.42	100.29
Sr	827.1	444.6	813.1	800.8	681.7	647	938	775	1182
Ba	2100	639	1697.5	1138	1209.6	734	2970	1203	950
Rb	90.2	188.8	68.8	81.8	71	58	86	73	93
Th	13	11.1	8.7	7.1	7.1	7.44	19.8	5.8	15.8
U	2.2	3.1	0.8	1	0.8	3.45	5.46	1	2.76
Ga	21.1	22.4	22.1	23.4	22.4	18	23	20	24
Zr	146.7	117.3	249.5	215.9	234	80	365	85	226
Hf	4.3	3.4	6.6	5.7	5.9	2.6	9.2	2.8	6.1
Y	14	15.2	10.7	8	12.2	28.5	31.9	27	28.7
Nb	6.9	13.4	6.8	5.4	7.5	7.4	17.3	6	8.2
Ta	0.5	0.8	0.2	0.3	0.3	0.4	1.1	0.3	0.85
La	59.1	42.3	42.3	31.1	41.1	53.4	86.7	43.5	70.4
Ce	128.7	90.2	88.4	66.6	89.1	108	169	108	148
Pr	14.2	10.24	10.98	7.55	10.74	13.3	19.8	13.3	18.7
Nd	53.2	40	42.8	29.8	40.4	55.5	77.8	55.8	75.2
Sm	7.86	6.12	6.52	4.39	6.2	10.1	12.8	11.3	12.9
Eu	1.18	1.06	1.45	1.19	1.54	3.1	3.37	2.9	3.22
Gd	4.21	4.32	3.66	2.73	4.14	7.84	9.45	8.3	9.02
Tb	0.54	0.58	0.47	0.35	0.56	1.07	1.18	1.2	1.21
Dy	2.57	2.68	2.05	1.66	2.24	5.57	6.19	5.8	5.73
Ho	0.4	0.47	0.32	0.27	0.35	1.01	1.06	1	1.02
Er	1.11	1.34	0.84	0.74	1.03	2.75	2.91	2.7	2.95
Tm	0.17	0.2	0.11	0.11	0.14	0.357	0.4	0.36	0.37
Yb	0.99	1.19	0.68	0.65	0.9	2.34	2.64	2.1	2.26
Lu	0.14	0.17	0.1	0.1	0.14	0.33	0.39	0.27	0.3
ASI	1.15	1.427	1.1	1.2	1.194	0.963	1.006	0.724	0.939
#mg	0.53	0.63	0.42	0.41	0.41	0.61	0.42	0.67	0.58
Na_2O/K_2O	1.34	0.62	1.85	1.8	1.91	0.69	0.64	0.41	0.61
Rb/Sr	0.109	0.425	0.085	0.102	0.104	0.09	0.092	0.094	0.079
Nd/Th	4.092	3.604	4.92	4.197	5.69	7.46	3.929	9.621	4.759
ΣREE	274.37	200.87	200.68	147.24	198.58	264.66	393.69	256.53	351.28
Eu/Eu*	0.627	0.63	0.907	1.051	0.929	1.065	0.937	0.915	0.913
Ce_N/Yb_N	35.818	20.884	35.818	28.231	27.277	12.717	17.638	14.17	18.043

Explanations: *GH* hybrid granitoids, *H* hybrids showing ocellar textures, *D* hybrid diorites

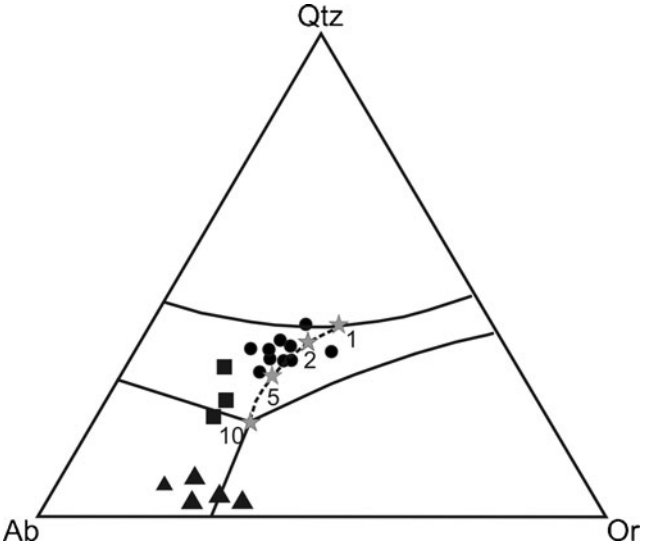

Fig. 6 Plot of the hybrid rocks composition in the Qtz-Ab-Or compositional space. Stairs—the melting minima for 1, 2, 5 and 10 kbar of pressure and water under-saturated conditions (after Holtz and Johannes 1991); circles—hybrid granitoids; squares—hybrids showing ocellar texture; triangles—hybrid quartz-diorites (after Gawęda et al. 2005)

Eleven LA-MC-ICP-MS measurements on seven zircon crystals from the same rock (SP2) were made (Table 9). All data points are concordant within the assigned error (Fig. 11). Nine analyses from the oscillatory-zoned zircon zones yield a concordia age of 368±8 Ma (MSWD=1.1). Two data points from inherited cores give a concordia age of ca. 530 Ma.

Discussion

The Western Tatra granitoids were previously interpreted as typical S-type granites (Poller et al. 2001a). The textures found in the analysed rocks advocate that mixing and mingling of magmas of different chemistry occurred during the granitoid magma emplacement. The presence of mafic clots and associated micrographic intergrowths at the border zone between the mafic and felsic portions suggest the clots have originated in mafic magma and cooled relatively quickly. Quenching is thought to be a process responsible for the acicular apatite formation, both in the matrix and as the inclusions in feldspars (Hibbard 1991; Baxter and Feely 2002). Anorthite spikes in plagioclases are also interpreted in terms of felsic and mafic magma mixing, as well as titanite-feldspar ocelli. The zoned allanite-epidote crystals (Fig. 3b) are typical of mafic, oxidised magmas (Broska and Uher 1991). The high content of Ba in fine-grained matrix K-feldspar crystal and their inverted chemical zonation might be also attributed to magma mixing (Long and Luth 1986; Słaby and Götze 2004). Hornblende and biotite rimmed quartz ocelli are explained as the result of magma mixing, taking place during the crystal nucleation (Hibbard 1991; Baxter and Feely 2002), i.e. rather early in the granitoid magma history.

The internally zoned alkali feldspar megacrysts, with inclusion zones, resorption and sporadically discontinuous albite mantling might be a result of both sub-isothermal

Table 7 Temperature and pressure calculations

Pressure S (1992)	Temperature B & H (1990)	Temperature V (1991)	Temperature G (2009)	Temperature F & L (1988); N & B (1987)
4.6 kbar	697	767	698	695
5.3 kbar	712	786	723	720
5.5 kbar	728	792	731	724
6.0 kbar	739	805	747	730
6.1 kbar	791	808	752	738

Explanations: *S* Schmidt (1992), *B & H* Blundy and Holland (1990), *V* Vyhnal et al. (1991), *G* Gawęda (2009), Fuhrman and Lindsley (1988), Nekvasil and Burnham (1987)

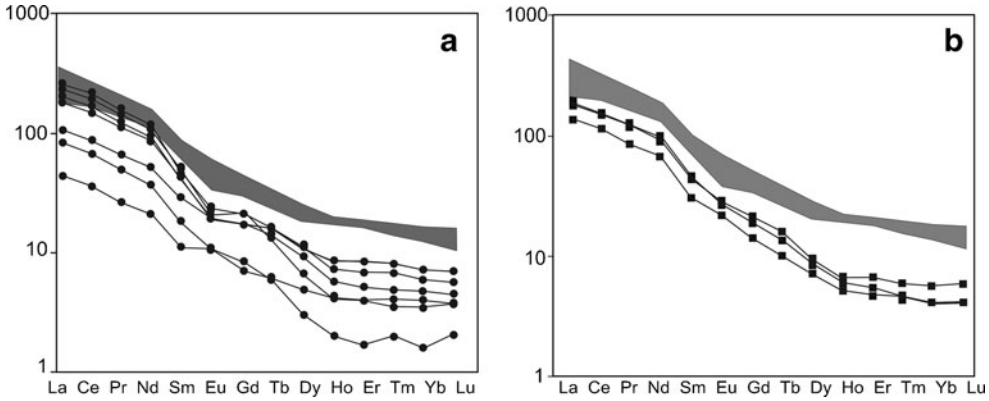

Fig. 7 Rare earth elements patterns, normalized to C1 chondrite (after Sun and McDonough 1989), in hybrid granites **a** and in ocellar rocks **b**. The shaded area shows the range of REE patterns of quartz-diorites from the Tatra Mountains (after Gawęda et al. 2005)

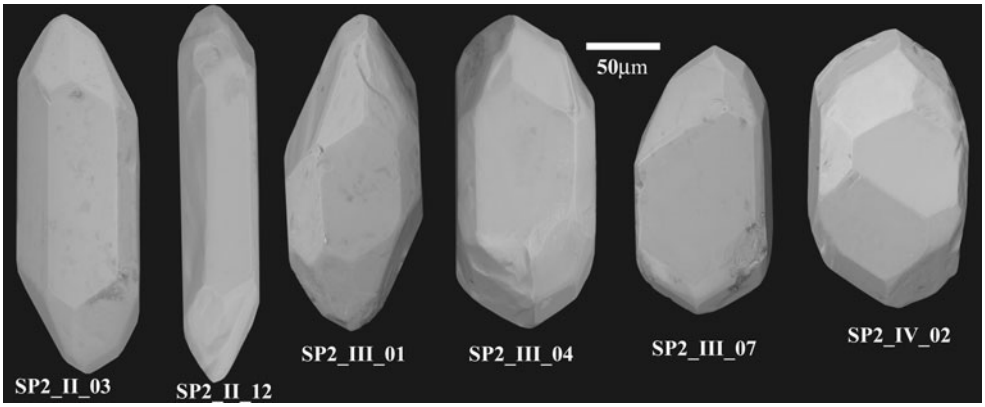

Fig. 8 Secondary electron (SE) images of zircon crystals from hybrid granitoid showing ocellar textures (sample SP2). Descriptions of zircons are included in the text

decompression (Nekvasil 1991, Eklund and Shebanov 1999) and mafic and felsic magma mixing (e.g. Hibbard 1991, Słaby and Götze 2004).

The linear trends observed in variation diagrams for hybrid granites and quartz-diorites (Figs. 5a-i) indicate mixing as a predominant factor governing the evolution of the magma. Although the quartz-diorites are hybrid rocks, fractionation was also shown to have occurred in their parent magma (Gawęda et al. 2005), in contrast to the hybrid granites where no fractionation trend was noted.

Nd and Th are thought to be elements representing contrasting magmatic sources: Nd enrichment is typical of mantle derived magmas while Th is enriched in those derived from the upper crust. The Nd versus Th brings the important information about the hybrid rocks position (Fig. 5j). Most of hybrid granitoids and some diorites form one trend with Nd/Th=2–4, suggesting an interplay between monazite-bearing crustal rocks and mantle-derived magma (Bea et al. 1999). Two quartz-diorite samples and ocellar titanite-rich hybrids are Nd-enriched (Nd/Th=4–9), suggesting predominance of mantle component, while the two other hybrids plot as Th-rich (Nd/Th= 1.9-2.5), representing the crustal-dominated component (Table 5 and 6; Fig. 5j). Those observations are consistent with the suggestions of Poller et al. (2000), based on the Sr, Nd and Pb isotopic composition, pointing out the slab break-off model and mantle plume for the generation of diorite magma.

Relative to the quartz diorites the hybrid granitoids show lower total REE content and LREE enrichment (expressed as Ce_N/Yb_N). The negative Eu anomaly is typical of granites crystallizing under reduced conditions. K-feldspars are common carriers of Eu, causing the positive Eu anomaly in one porphyritic granitoid. The ocellar titanite-rich hybrids show chondrite-normalized REE patterns transitional between granitoids and diorites, with Eu/Eu*~1, which suggests more oxidizing conditions and a mantle influence (Table 5 and 6; Fig. 6).

Based on zircon typology, these granitoid samples are classified as hybrid calc-alkaline series granitoids (Group-4 of Pupin 1980; Fig. 9). CL images of the investigated zircons reveal domination of euhedral crystals with fine to medium-scale oscillatory zoning. In the early stages of growth [121] pyramids predominate, typical of crystals from granitoids with dominantly S-type characteristics. Then, the morphology of crystals changes, favouring [101] pyramids, common in hybrid-type granitoids (e.g. Pupin 1980; Schermaier et al. 1992; Köksal et al. 2008). The occurrence of oscillatory zoning of Hf in zircons suggests heterogeneities in the crystallization environment, or repeated fluctuations of the Hf concentration in the magma during zircon growth (e.g. Benisek and Finger 1993). This might be a result of rapid change in chemical conditions at the latest stages of crystallization, caused by the influx of new magma and consequently, may be related to magma mixing/mingling processes. The presence of intermittent dissolution surfa-

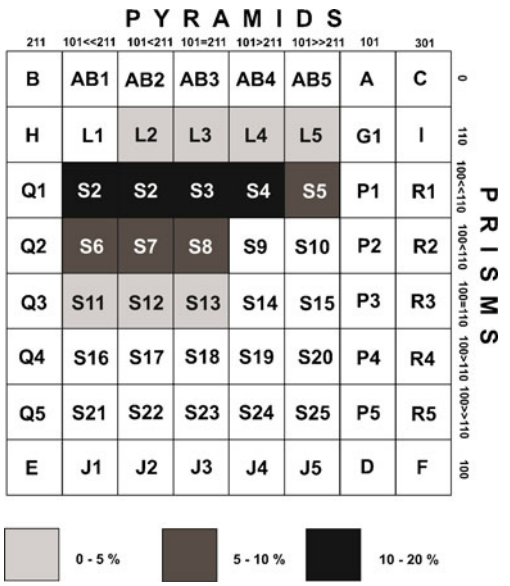

Fig. 9 Distribution of morphological types of zircon from hybrid granitoid with ocellar textures (sample SP2) on Pupin's (1980) diagram

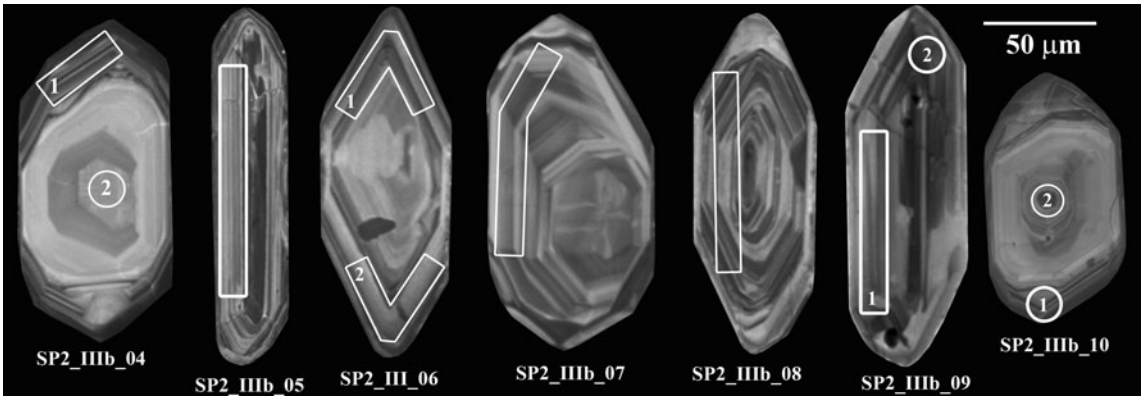

Fig. 10 Cathodoluminescence (CL) images of zircon crystals from hybrid granitoid with ocellar textures (sample SP2). Grains no. 5, 6, 7, 8 and 9 show magmatic oscillatory zoning from centre to margin. Grains no. 1 and 10 contain an older core surrounded by a younger rim with oscillatory zoning. The white lines show the approximate locations of laser ablation trenches and are not to scale. Analyses from the oscillatory-zoned zircon zones yield a concordia age of 368±8 Ma. Two data points from inherited cores give a concordia age of ca. 530 Ma (Fig. 11; Table 9)

ces between well-developed oscillatory zoning (Fig. 10) also supports this suggestion.

An overall enrichment in P and Y from core to rim is observed in analysed zircons (Table 8). The xenotime substitution in zircon is obviously constrained by the availability of Y and P in the magma. Therefore, the crystallization of apatite of mixed morphologies with respect to zircon (in the absence of monazite) is the key factor. Only if some P is still available after the complete crystallization of P-bearing minerals (apatite), it can enter into zircon in significant amounts (Caironi et al. 2000).

U-Pb isotopic data obtained by LA-MC- ICP-MS analyses of oscillatory growth-zones (Fig. 10) yield a concordia age of 368±8 Ma (2 sigma; Fig. 11). This age is interpreted as

Table 8 Microprobe analyses of selected zircon crystals from hybrid granitoids showing ocellar textures (sample SP2 (in wt% oxides)

Zircon crystals	P_2O_5	SiO_2	TiO_2	ZrO_2	HfO_2	ThO_2	UO_2	Sc_2O_3	Y_2O_3	Yb_2O_3	Total	Zr/Hf
SP2_IV_01/1c	0.18	31.84	0.02	66.48	1.33	0.03	0.03	0.04	0.10	0.02	100.07	44
SP2_IV_01/2r	0.13	31.71	0.04	67.08	1.39	0.00	0.05	0.02	0.00	0.00	100.43	42
SP2_IV_01/3r	0.10	31.96	0.00	67.42	1.66	0.00	0.06	0.00	0.00	0.02	101.26	35
SP2_IV_03/1r	0.13	31.85	0.01	66.72	1.08	0.10	0.02	0.03	0.09	0.02	100.06	54
SP2_IV_03/2r	0.13	31.63	0.00	67.44	1.10	0.02	0.05	0.00	0.01	0.02	100.39	54
SP2_IV_03/3r	0.18	31.31	0.05	66.63	1.13	0.00	0.04	0.04	0.10	0.04	99.52	52
SP2_IV_04/1c	0.13	31.90	0.01	67.50	1.28	0.00	0.00	0.00	0.00	0.01	100.82	46
SP2_IV_04/2c	0.13	31.69	0.00	67.58	1.27	0.00	0.00	0.02	0.00	0.02	100.73	46
SP2_IV_04/3c	0.11	31.55	0.06	65.83	2.23	0.06	0.07	0.03	0.01	0.00	99.94	26
SP2_IV_02/1c	0.13	31.97	0.03	66.73	1.20	0.00	0.05	0.02	0.00	0.10	100.22	49
SP2_IV_02/2r	0.06	31.95	0.00	66.62	1.25	0.00	0.03	0.00	0.00	0.08	100.00	47
SP2_IV_02/3r	0.12	31.96	0.00	67.24	1.25	0.00	0.01	0.00	0.00	0.01	100.59	47
SP2_III_04/1c	0.11	32.00	0.02	66.28	1.14	0.00	0.03	0.02	0.00	0.02	99.60	51
SP2_III_04/2r	0.10	31.46	0.01	66.55	1.46	0.04	0.04	0.01	0.02	0.00	99.70	40
SP2_III_04/3r	0.07	31.00	0.02	66.21	1.57	0.00	0.10	0.00	0.01	0.01	98.97	37
SP2_III_01/1c	0.12	31.85	0.00	66.96	1.30	0.04	0.00	0.02	0.00	0.00	100.29	45
SP2_III_01/2r	0.05	31.00	0.00	67.19	1.37	0.00	0.04	0.00	0.00	0.06	99.71	43
SP2_III_06/1r	0.22	32.01	0.00	66.23	1.22	0.00	0.10	0.07	0.28	0.05	100.18	47
SP2_III_06/2r	0.15	31.53	0.00	66.90	1.10	0.03	0.00	0.06	0.20	0.05	100.02	53
SP2_III_06/3r	0.13	31.52	0.00	66.85	1.18	0.06	0.07	0.07	0.13	0.05	100.06	49
SP2_III_06/4r	0.21	31.04	0.00	66.69	1.21	0.00	0.10	0.08	0.29	0.02	99.68	48

Explanations: *c* cores, *r* rims

Table 9 LA-MC-ICP-MS U-Pb zircon data from hybrid granitoid with ocellar textures (sample SP2)

File name	Final blank corrected intensities				Final common Pb corrected ratios								
	$^{204}Pb^{*}$	$^{206}Pb^{*}$	$^{207}Pb^{*}$	$^{238}U^{\#}$	$^{206}Pb/^{204}Pb$	2RSE (%)	$^{207}Pb/^{235}U$	2RSE (%)	$^{206}Pb/^{238}U$	2RSE (%)	Rho	$^{207}Pb/^{206}Pb$	2RSE (%)
SP2_III_04/1	3.49	3397	229	126	1385	53.0	0.45	11.7	0.05	53.6	0.58	0.06	53.2
SP2_III_04/2	1.02	3381	164	42	8439	12.3	0.68	16.4	0.09	16.4	0.51	0.06	13.6
SP2_III_05	1.34	398	29	15	414	67.7	0.42	15.7	0.05	13.4	0.38	0.05	7.8
SP2_III_06/1	1.11	938	64	34	958	48.4	0.45	10.6	0.06	9.3	0.16	0.06	5.5
SP2_III_06/2	1.10	358	29	16	536	27.4	0.45	6.0	0.06	27.6	0.48	0.06	27.5
SP2_III_07	1.21	208	17	9	249	30.3	0.42	6.6	0.05	30.3	0.38	0.06	30.3
SP2_III_08	0.93	385	24	14	865	67.5	0.42	14.8	0.06	13.0	0.15	0.05	7.6
SP2_III_09/1	0.90	500	41	22	768	29.8	0.43	6.5	0.06	29.8	0.30	0.06	29.8
SP2_III_09/2	0.78	785	53	28	1045	30.0	0.44	6.6	0.06	5.8	0.14	0.05	3.4
SP2_III_10/1	0.31	245	16	9	790	92.9	0.45	21.3	0.05	17.9	0.18	0.06	10.6
SP2_III_10/2	0.52	294	21	7	1307	81.6	0.68	17.9	0.08	15.9	0.58	0.06	9.2

Explanations: * final blank corrected intensities in μV, # final blank corrected intensities in mV

reflecting the time of zircon formation during a magmatic event.

Only a few crystals have subhedral cores. These are interpreted as xenocrysts, probably inherited from the crustal source-rocks of the magma. The zircon cores yield an age of ca. 530 Ma which reflect their crystallization age. A similar inherited zircon age signature was found in paragneisses (Kohút et al. 2008) and in orthogneisses from the crystalline basement of the Tatra Mountains (Burda and Klötzli 2010) as well as from another crystalline complexes from the Central Western Carpathians (e.g. Putiš et al. 2008; Putiš et al. 2009). The presence of these oldest meta-magmatic rocks in the Western Tatra Mts. could be linked to the fragmentation of the northern margin of Gondwana (Burda and Klötzli 2010).

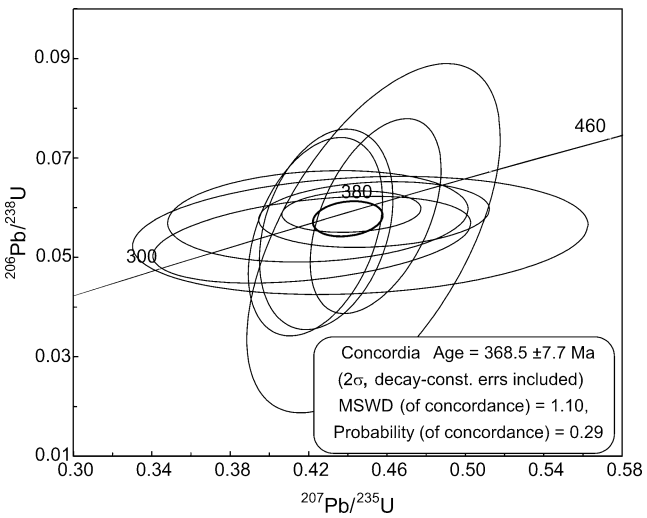

Fig. 11 Concordia plots of LA-MC-ICP-MS U-Pb zircon analytical results from the oscillatory-zoned zircon zones from hybrid granitoids showing ocellar textures (sample SP2)

The mixing-mingling of felsic and mafic magmas, predating the main granite intrusion and influencing the development of the Western Tatra granite, sheds new light on the origin of this granitoid body. The Western Tatra granite, previously interpreted as purely S-type, is in fact a composite pluton, showing common features with the I/S High Tatra granite portion. The age of the hybrid rocks from the Western Tatra Mountains marks subduction processes at the Laurussia margin followed by the collision of microterranes, and finally of the Gondwana promontory.

Conclusions

1. Granitoids from the Western Tatra Mts., interpreted previously as the products of crystallization from purely S-type melts, represent in fact hybrid melts.
2. LA-MC-ICP-MS U-Pb zircon age calculations (368± 8 Ma) indicate an Early Variscan magmatic episode. As the 368 Ma age is found in zircon rims it could be interpreted as the oldest Variscan magmatic event in that part of the Tatra Mountains.
3. Textural features, together with mineralogy and chemistry, point out the presence of mixing/mingling phenomena, which started from early stages of magma evolution. The vast distribution of textures generated by mingling-mixing processes, together with the rocks chemistry, suggests that these processes governed the formation of the Western Tatra granitoid pluton.
4. The hybridization event defined here, which predates the main magmatic activity in the Tatra Mountains, provides new insight into the paleotectonic reconstructions of the Early Variscan realm in the Western Carpathians.

Acknowledgements The Polish Ministry of Sciences and Higher Education sponsored the investigations, by MNiSW grant No. 2 P04D 003 29 (given for JB) and MNiSW grant No. N 307 027837 (given for AG). Additional funds from Austrian Science Fund FWF (START project 267-N11 and project P18202-N10 given for UK) is deeply acknowledged.

Ewa Teper is thanked for the assistance during CL investigations, while Lidia Jeżak and Piotr Dzierżanowski are acknowledged for the help during microprobing.

The authors would like to thank Sadhbh Baxter and M. Cemal Göncüoglu who provided detailed and useful reviews of the manuscript as well as Andreas Möller for careful editorial handling.

References

Bac-Moszaszwili M (1996) The uplift of the Tatra massif in Tertiary and Quaternary. In: The Tatra National Park—Nature and man. Zakopane, Oct. 6th–9th 1995, Conference proceedings: pp 68–71

Baxter S, Feely M (2002) Magma mixing and mingling textures in granitoids: examples from the Galway Granite, Connemara, Ireland. Mineral Petrol 76:63–74

Bea F, Montero P, Molina F (1999) Mafic precursors, peraluminous granitoids, and late lamprophyres in the Avila batholith: a model for the generation of Variscan batholiths in Iberia. J Geol 107:399–419

Benisek A, Finger F (1993) Factors controlling the development of prism faces in granite zircons: a microprobe study. Contrib Miner Petrol 114:441–451

Blundy JD, Holland TJB (1990) Calcic amphibole equlibria and a new amphibole-plagioclase geothermometer. Contrib Miner Petrol 104:208–244

Broska I, Uher P (1991) Regional typology of zircon and its relationship to allanite/monazite antagonism (on an example of Hercynian granitoids of Western Carpathians). Geol Carpath 42:271–278

Burda J (2010) Internal structures and dating of complex zircons from High Tatra massif granodiorites, Poland. 10th International conference -Methods of absolute chronology- 22–25 April Gliwice, Poland. Abstracts & Programme 79

Burda J, Klötzli U (2007) LA-MC-ICP-MS U-Pb zircon geochronology of the Goryczkowa type granite—Tatra Mts., Poland. Pol Tow Miner Pr Spec 31:89–92

Burda J, Klötzli U (2010) Pre-Variscan evolution of the Western Tatra Mts., Poland: new insights from U-Pb zircon dating. 20th General Meeting of the International Mineralogical Association, 21–27 August Budapest, Hungary. Acta Mineral Petrogr Abstr Ser. Szeged 6: p 449

Caironi V, Colombo A, Tunesi A, Gritti C (2000) Chemical variations of zircon compared with morphological evolution during magmatic crystallization: an example from the Valle del Cervo Pluton (Western Alps). Eur J Miner 12:779–794

Didier J, Barbarin B (1991) Enclaves and granite petrology: developments in petrology 13. Elsevier, Amsterdam

Eklund O, Shebanov AD (1999) The origin of rapakivi texture by subisothermal decompression. Precambrian Res 95:129–146

Fuhrman ML, Lindsley DH (1988) Ternary-feldspar modeling and thermometry. Am Miner 73:201–215

Gawęda A (2008) Apatite-rich enclave in the High Tatra granite, Western Carpathians: petrological and geochronological study. Geol Carpath 59(4):295–306

Gawęda A (2009) Enclaves in the High Tatra Granite. University of Silesia publishing House, Monographic series, Katowice: 180 pages (in Polish, English abstract)

Gawęda A, Doniecki T, Burda J, Kohút M (2005) The petrogenesis of quartz-diorites from the Tatra Mountains (Central Western Carpathians): an example of magma hybridisation. N Jb Miner Abh 181(1):95–109

Harrison TM, Watson EB (1983) Kinetics of zircon dissolution and zirconium diffusion in granitic melts of variable water content. Contrib Miner Petrol 84:67–72

Hibbard MJ (1991) Textural anatomy of twelve magma-mixed granitoid systems. In: Didier J, Barbarin B (eds) Enclaves and granite petrology. Elsevier, Amsterdam, pp 431–444

Holtz F, Johannes W (1991) Genesis peraluminous granites I. Experimental investigation of melt compositions at 3 and 5 kb and various H_2O activities. J Petrol 32:935–958

Klötzli U, Klötzli E, Günes Z, Košler J (2009) External accuracy of laser ablation U-Pb zircon dating: results from a test using five different reference zircons. Geostand Geoanal Res 33(1):5–15

Kohút M, Janak M (1994) Granitoids of the Tatra Mts., Western Carpathians: field relations and petrogenetic implications. Geol Carpath 45(5):301–311

Kohút M, Poller U, Gurk C, Todt W (2008) Geochemistry and U-Pb detrital zircon ages of metasedimentary rocks of the Lower Unit, Western Tatra Mountains (Slovakia). Acta Geol Pol 58:371–384

Köksal S, Cemal Göncüoglu M, Toksoy-Köksal F, Möller A, Kemnitz H (2008) Zircon typologies and internal structures as petrogenetic indicators in contrasting granitoid types from central Anatolia, Turkey. Mineral Petrol 93:185–211

Long PE, Luth WC (1986) Origin of K-feldspar megacrysts in granitic rocks: Implication of a partitioning model for barium. Am Miner 71:367–375

Ludwig KR (2003) Isoplot/Ex version 3.00. A geochronological toolkit for Microsoft Excel. Berkeley Geochronology Center. Special Publication No. 4

Menéndez M, Ortega LA (1999) Evidence of magmatic hybridization related with feeding zones: the synkinematic Guitiriz granitoid, NW Iberian Massif. Geological Society, London, Special Publications 168:pp 255–272

Morozewicz K (1914) Über die Tatragranite. N Jhb Miner Geol Paläont 39:289–345

Nekvasil H (1991) Ascent of felsic magmas and formation of rapakivi. Am Miner 76:1279–1290

Nekvasil H, Burnham CW (1987) The calculated individual effects of pressure and water content on phase equilibria in the granite system. In: Mysen BO (ed) Magmatic processes: physicochemical principles. Geochemical Society, University Park, pp 433–445

Poller U, Janak M, Kohút M, Todt W (2000) Early Variscan magmatism in the Western Carpathians: U-Pb zircon data from granitoids and orthogneisses of the Tatra Mountains, Slovakia. Int J Earth Sci 89:336–349

Poller U, Todt W, Kohút M, Janak M (2001a) Nd, Sr, Pb isotope study of the Western Carpathians: implications for the Paleozoic evolution. Schweiz Miner Petrol Mitt 81:159–174

Poller U, Huth J, Hoppe P, Williams IS (2001b) REE, U, Th and Hf distribution in zircon from Western Carpathian Variscan granitoids: a combined cathodoluminescence and ion microprobe study. Am J Sci 301:858–876

Pupin JP (1980) Zircon and granite petrology. Contrib Mineralog Petrol 73:207–220

Putiš M, Sergeev S, Ondrejka M, Larionov A, Siman P, Spisiak J, Uher P, Paderin I (2008) Cambrian-Ordovician metaigneous rocks associated with Cadomian fragments in the West-Carpathian basement dated by SHRIMP on zircons: a record from the Gondwana active margin setting. Geol Carpath 59(1):3–18

Putiš M, Ivan P, Kohút M, Spišiak J, Siman P, Radvanec M, Uher P, Sergeev S, Larionov A, Méres Š, Rastislav Demko R, Ondrejka M (2009) Meta-igneous rocks of the West-Carpathian basement, Slovakia: indicators of Early Paleozoic extension and shortening events. Bull Soc Géol Fr 180(6):461–471

Schermaier A, Haunschmid B, Schubert G, Frasl G, Finger F (1992) Diskriminierung von S-Typ und I-Typ Graniten auf der Basis zirkontypologischer Untersuchungen. Frankf geiwiss Arb Serie A 11:149–153

Schmidt MW (1992) Amphibole equilibria in tonalite as a function of pressure: an experimental calibration of the Al-in-hornblende barometer. Contrib Miner Petrol 110:304–310

Słaby E, Galbarczyk-Gąsiorowska L (2002) Barium In alkali feldspar megacrysts from Szklarska Poręba Huta porphyritic granite-possible indicator of magma mixing. Mineralog Pol Spec Pap 20:198–201

Słaby E, Götze J (2004) Feldspar crystallization under magma-mixing conditions shown by cathodoluminescence and geochemical modelling—a case study from the Karkonosze pluton (SW Poland). Miner Mag 68:541–557

Słaby E, Galbarczyk-Gąsiorowska L, Seltmann R, Müller A (2007a) Alkali feldspar megacryst growth: geochemical modelling. Mineral Petrol 89:1–29

Słaby E, Seltmann R, Kober B, Müller A, Galbarczyk-Gąsiorowska L, Jeffries T (2007b) LREE distribution patterns in zoned alkali feldspar megacrysts—implication for parental melt composition. Miner Mag 71:193–217

Slàma J, Košler J, Schaltegger U, Tubrett M, Gutjahr M (2006) New natural zircon standard for laser ablation ICP-MS U-Pb geochronology. Abstract WP05. Winter Conference on Plasma Spectrochemistry, Tucson, pp 187–188

Speer JA (1982) Zircon. Rev Miner 5:67–112

Stacey JS, Kramers JD (1975) Approximation of terrestrial lead isotope evolution by a two stage model. Earth Planet Sci Lett 26:207–221

Sun SS, McDonough WF (1989) Chemical and isotopical systematics of oceanic basalts: implications for mantle composition and processes. Magmatism in the Oceanic Basins. Geol Soc Spec Publ 42:313–345

Vavra G (1990) On the kinematics of zircon growth and its petrogenetic significance: a cathodoluminescence study. Contrib Miner Petrol 106(1):90–99

Vernon RH (2004) A practical guide to rock microstructure. Cambridge University Press: Chapter 3.

Vernon RH, Paterson SR (2008) How late are K-feldspar megacrysts in granites? Lithos 104:327–336

Vyhnal CR, McSween HY Jr, Speer JA (1991) Hornblende chemistry in southern Appalachian granitoids: implications for aluminum hornblende thermobarometry and magmatic epidote stability. Am Miner 76:176–188

Whitney DL, Evans BW (2010) Abbreviations for names of rock-forming minerals. Am Miner 95:185–187

Wiebe RA (1968) Plagioclase stratigraphy: a record of magmatic conditions and events in a granite stock. Am J Sci 266:690–703

Wiedenbeck M, Alle P, Corfu F, Griffin WL, Meier M, Oberli F, Von Quadt A, Roddick JC, Spiegel W (1995) Three natural zircon standards for U-Th-Pb, Lu-Hf, trace element and REE analyses. Geost Newslet 19:1–23